Physics of Plasmas

Test particle dynamics in low-frequency tokamak turbulence

Cite as: Phys. Plasmas **26**, 102301 (2019); https://doi.org/10.1063/1.5115231
Submitted: 15 June 2019 . Accepted: 12 September 2019 . Published Online: 01 October 2019

J. Médina, M. Lesur, E. Gravier, T. Réveillé, and P. Bertrand

Test particle dynamics in low-frequency tokamak turbulence

Cite as: Phys. Plasmas **26**, 102301 (2019); doi: 10.1063/1.5115231
Submitted: 15 June 2019 · Accepted: 12 September 2019 ·
Published Online: 1 October 2019

View Online Export Citation CrossMark

J. Médina, M. Lesur, E. Gravier, T. Réveillé, and P. Bertrand

AFFILIATIONS

Université de Lorraine, CNRS, IJL, F-54000 Nancy, France

ABSTRACT

We study the evolution of one million test particles in a turbulent plasma simulation, using the gyrokinetic code Trapped Element REduction in Semi-Lagrangian Approach (TERESA), as a method to get insights into the type of transport governing the plasma. TERESA (Trapped Element REduction in Semi-Lagrangian Approach) is a collisionless global 4D code which treats the trapped particles kinetically, while the passing particles are considered adiabatic. The Vlasov-Poisson system of equations is averaged over the cyclotron and the trapped particle's bounce motion, and thus, the model focuses on slow phenomena of the order of the toroidal precession motion of the banana orbits. We initialize the test particles, which are de facto "test banana-centers," at a time of the simulation when the plasma is turbulent. We impose an initial temperature and density gradients, and only the Trapped Ion Mode (TIM) instability can develop in this system. We then calculate the Mean Squared Displacement of the test particles as a function of time in order to obtain a random walk diffusion coefficient. We observe that the radial diffusion of the test particles depends on their toroidal precession kinetic energy (E), in such a way that the transport of particles is dominated by a strong, relatively narrow peak at the resonant energies. A radial particle diffusion flux is then calculated and compared to the total radial particle flux accounting for all the transport processes such as diffusion and advection which is obtained directly from the TERESA code. We can thus compare the diffusive contribution to the particle flux against the nondiffusive contributions. The results show that the total flux is essentially diffusive which is consistent with our simulation setup aiming for "global turbulence." Both fluxes present a peak around a resonance energy $E_R \approx 1.74 T_i$ between the TIM and the particles. Both thermal and high-energy particles do not contribute significantly to radial transport.

I. INTRODUCTION

Understanding, predicting, and mitigating turbulent transport in tokamaks are some of the main challenges to overcome in order to achieve commercially viable fusion reactors.

Turbulent transport processes include diffusion,[16,23,27,35] subdiffusion,[9,37,38] or superdiffusion[42] appearing in fusion scenarios such as predisruptive phases, toroidicity-induced Alfvén eigenmode (TAE) transport or saturated tearing modes, convection,[1,2,11,27] and ballistic events such as avalanches.[11,26,36,39,41,43]

Although there is no global theory of turbulence, tremendous progress on this subject has been made in the last few decades, thanks to a combination of analytical, experimental, and numerical research.[17] Recently, the field of High Performance Computing (HPC) combined with advances in gyrokinetic theory[3] opened new horizons in the domain of numerical simulations of turbulence,[18] allowing for a deeper understanding of transport. The gyrokinetic framework allows us to simulate high-temperature plasma behavior, usually in a 5 dimensional space, by averaging out the fast cyclotron motion of the charged particles. Simulation codes based on this model nonexhaustively include GYSELA,[8,12,21,22,41] GENE,[13,20,28] GKW,[34] ELMFIRE,[24] ORB5,[29] GT5D,[25,26] and GYRO.[4,5]

It is possible to further reduce the model by averaging out, in addition to the cyclotron motion, the trapped particle bounce (or banana) motion and considering adiabatic passing particles with kinetic trapped ions (from zero to suprathermal, although nonrelativistic, energies), thus focusing on slow phenomena on a time scale of the toroidal precession of trapped particles with thermal velocity, which is around 10^{-2} s. In this work, we use the trapped element reduction in semi-Lagrangian approach (TERESA) code[6,7,10,14,19,31,32,40] which is based on this reduced gyrokinetic model and which is less computationally intensive than standard gyrokinetic codes. This axisymmetric, electrostatic code solves the Vlasov equation coupled to the quasineutrality constraint, in a 4 dimensional space: 2 spatial variables (α, ψ) and 2 adiabatic invariants κ and E. $\alpha = \varphi - q\theta$ is the precession angle with φ the toroidal angle, θ the poloidal angle, and q the safety factor, taken independent of the radius. $\psi = \psi_0 - cr^2$ is the poloidal magnetic flux with r the radial coordinate, c a constant, and ψ_0 a shift so that $\psi = 0$ is toward the edge. $\kappa^2 = \sin^2(\frac{\theta_0}{2})$ is the trapping parameter with θ_0 the poloidal angle where the trapped particle parallel velocity changes the sign, μ the magnetic moment, and $E = \frac{1}{2}mv_\parallel^2 + \mu B$ the kinetic energy. Although the code allows the simulation of kinetic trapped ions and electrons,[15] in this work, we focus on kinetic trapped ions and consider the trapped electrons as a neutralizing background. The turbulence obtained in our simulation is driven by Trapped Ion Modes (TIMs), and we expect that mode-particle resonance plays an important role in the transport of particles and energy. The TERESA code allows for numerical investigation of fundamental phenomena and is not intended to give quantitative predictions for tokamaks.

Although this kind of code solves the distribution function f and the electric potential ϕ, it does not yield individual particle trajectories. Particles, momentum, and energy fluxes can be obtained from f and ϕ, but discriminating diffusive and convective processes typically requires convoluted methods such as dedicated dynamical synthetic experiments. Investigating the particle trajectories in the turbulent plasma would lead to have better insights into diverse phenomena occurring in tokamaks such as diffusion, hyper- or subdiffusion,[45] advection, ballistic motions, and the trapping of particles in potential wells. Indeed, the analysis can be done locally in space, within a short timespan and without ambiguity.

In this work, in order to have access to the particle trajectories, we add test particles to TERESA. Test particles are particles advected by the electrostatic field, but they do not affect it. They can thus be used as markers in the turbulent plasma, representing exactly the motion of a single particle belonging to f. The test particle trajectories are computed directly in the TERESA code, thus allowing for the same order of accuracy as solving f and ϕ directly.

The present work aims at distinguishing the radial diffusive flux of the test particles, which are de facto "banana-centers," from the total particle flux. We initialize 10^6 test particles in a TIM-driven, turbulent, core plasma and investigate their time-evolution and their statistical properties.

In Sec. II A, we describe briefly the bounce-averaged gyrokinetic model, and then, in Sec. II B, we explain our implementation of test particles in TERESA. In Sec. III, we detail our simulation parameters and the initialization of the test particles and give information on the turbulent plasma such as the time evolution of the dominant modes, the typical mode spectrum, and the absence of a large scale plasma structure. Then, in Sec. IV A, we analyze the time evolution of the test particle Mean Squared Displacement (MSD) in order to calculate a radial random walk diffusion coefficient in velocity space. With this diffusion coefficient, we estimate a radial diffusive flux in velocity space for the test particles in Sec. IV B, and we compare it to the total radial particle flux obtained from f and ϕ. In Sec. V, we draw our conclusions.

II. TEST PARTICLE IMPLEMENTATION IN THE TERESA CODE

A. A bounce averaged gyrokinetic model

The TERESA code[6,7,10,14,19,32,40] is based on a reduced electrostatic gyrokinetic model focusing on trapped particles, where the cyclotron and bounce motions are averaged out. TERESA does not aim to quantitatively predict the transport in the existing or future tokamaks. Instead, its purpose is to investigate the general trends and fundamental ingredients of turbulent transport in a qualitative way. In this paper, we focus on trapped hydrogen ions. The passing particles respond adiabatically to the electric potential, while the trapped ion motion is described kinetically using the Vlasov equation

$$\frac{\partial f}{\partial t} - [H, f]_{\alpha, e\psi} = 0. \qquad (1)$$

The trapped electrons are assumed as a neutralizing background. Equation (1) is coupled to the quasineutrality constraint

$$C_1\left[\phi + \mathcal{F}^{-1}\left(i\delta_m\hat{\phi}_m\right)\right] - C_2\bar{\Delta}\phi = \frac{2}{\sqrt{\pi}}\int_0^\infty \mathcal{J}_0(E)f\sqrt{E}\mathrm{d}E - 1, \qquad (2)$$

which comes from the fact that the fluctuation densities of the ions (passing + trapped) are locally equal to the fluctuation densities of the electrons. Here, we give a brief explanation of the model. More details on each term, as well as the normalization, can be found in Refs. 31 and 32. f is the ion "banana-center" (charged + e) distribution function. $H = E(1 + e\Omega_d\psi) + e\bar{\bar{\phi}}$ is the Hamiltonian of an ion banana-center, where Ω_d is linked to the precession frequency and $\bar{\bar{\phi}}(\alpha, \psi; \kappa, E)$ is the gyrobounce averaged electric potential felt by the banana center. $[H, f]_{\alpha, e\psi}$ are the Poisson brackets in the angle action (α, $e\psi$). A position in phase space is determined by α the toroidal precession angle, ψ the poloidal magnetic flux which serves as a radial coordinate, and two adiabatic invariants which are fixed parameters: E the particle kinetic energy present in the toroidal precession motion and κ the pitch angle. All quantities in the TERESA code are dimensionless and are normalized as follows: $\psi = \Psi/L_\psi$, where ψ is dimensionless, Ψ is the physical magnetic flux, and L_ψ is the radial length of the simulation box in magnetic flux units, E is normalized to ion temperature T_i, and $\phi = R_0 e\Phi/aT_i$, where Φ is the physical electric potential and a and R_0 are the minor and major tokamak radii, respectively.

The quasineutrality equation yields the electric potential $\phi(\alpha,\psi)$. The term $C_1\phi$ in the LHS accounts for the adiabatic response of the passing particles to ϕ. Although there is no collision in the model (thus no collisional transfer between passing and trapped particles), the term δ_m models the effects of electron-ion (every particles, trapped and passing) collisions as a phase shift between ϕ and the electron density.[31] $\mathcal{F}^{-1}$ is the inverse Fourier transform, $\hat{\phi}_m$ is the Fourier transform of ϕ in the α direction, and m is the α-mode label number. $\bar{\Delta}\phi$ is the polarization term accounting for the difference between the true density and the bounce-averaged density. $\mathcal{J}_0$ is the averaging operator, and C_1 and C_2 (the inverse aspect ratio) are the two fixed parameters. The RHS accounts for the difference between the trapped ions and trapped electron densities.

B. Test particles in TERESA

Test particles allow the study of, local or global, diffusion, advection, ballistic motion, trapped particles in potential wells. In order to obtain insights into the type of transport processes occurring in the simulation, we need to determine the banana-center trajectories. This information is not obtained by solving the system for f, and therefore, we will use the test particles, which are charged particles advected by the electric potential without affecting it and can thus be used as "markers" in the plasma.

There are multiple approaches to use test particles, and the main ones are as follows: (1) determining an electric potential map from analytical methods and letting the test particles evolve in it,[30] or (2) obtaining the electric potential map either from a kinetic simulation (or experimental measurements[33,44]) and determining the test particle trajectories in post processing, or (3) solving the test particle trajectories directly in the kinetic simulation.

Method 1 offers the main advantage that it does not require large computational power but it relies on a predetermined analytical description of the electric potential configuration.

Method 2 is usually more computationally intensive as it generally requires a nonlinear kinetic simulation. One downside is that the test particle trajectories which are solved in post processing are not solved at the same order of precision than the simulation: $\Delta t \ll dt$, where Δt is the kinetic simulation time step and dt the post processed test particle trajectory time step. Although it is in principle possible to use method 2 with $\Delta t = dt$ and obtain method 3, we distinguish method 2 from method 3 because it would require the saving of the potential map at each dt and would thus be prohibitively expensive in terms of numerical storage.

In this work, we will use method 3 which has the advantage of giving the test particle trajectories with the same order of precision as the numerical scheme of the TERESA simulation ($\Delta t = dt \sim 10^{-6}\Omega_d^{-1}$) but with the downside of being more expensive in terms of computational time and numerical storage. With one million test particles, the TERESA simulation usually takes twice as much time than without test particles.

The test particle trajectories follow the Vlasov characteristics, and as we have $\frac{df}{dt} = 0$ over particle trajectories, the test particles follow the contours of constant f in time. The test particle dynamics is described by the characteristic equations:

$$\dot{\alpha} = \frac{1}{e}\frac{\partial H}{\partial \psi} = E\Omega_d + \frac{\partial \bar{\bar{\phi}}}{\partial \psi}(\alpha, \psi; \kappa, E), \tag{3}$$

and

$$\dot{\psi} = -\frac{1}{e}\frac{\partial H}{\partial \alpha} = -\frac{\partial \bar{\bar{\phi}}}{\partial \alpha}(\alpha, \psi; \kappa, E). \tag{4}$$

These positions are solved at each time step using the RK4 method, and they depend on the energy parameter E. The test particle energy E conservation throughout the simulation is at the same order of accuracy than other quantities in TERESA. At each time step of the simulation, TERESA thus solves f, ϕ, and the test particle positions in phase space.

III. SIMULATION CONFIGURATION

The bounce-averaged gyrokinetic code TERESA allows us to simulate a fusion plasma core on the precession time scale, in a qualitative way, and at the same time follow test particle trajectories in this plasma. We use a uniform grid in phase space: N_ψ points in $\psi \in [0; 1]$, where $\psi = 1$ is the center of a poloidal section and $\psi = 0$ is toward the edge (but still fulfilling core plasma conditions) and N_α points in the toroidal precession angle $\alpha \in [0; 2\pi[$. The number of points is $N_\alpha \times N_\psi = 2045 \times 1025$. For the energy E, we choose a non-uniform grid spacing with the introduction of a new parameter $V = \sqrt{E}$, with $N_V = 96$ points. The range $E \in [0; 20]$ is chosen to allow good convergence of simulation results. For the κ adiabatic invariant, we only use a single value which forces the trapped particles to be deeply trapped. We recall the grid configuration in Table I.

TABLE I. Grid used for our simulation. α and ψ are the phase-space variables, while κ and E (or V) are parameters.

Grid	Number of grid points	Value
α	$N_\alpha = 2045$	$\alpha \in [0; 2\pi[$
ψ	$N_\psi = 1025$	$\psi \in [0; 1]$
κ	$N_\kappa = 1$	$\kappa = 0$
E,V	N_E or $N_V = 96$	$E \in [0; 20]$

For boundary conditions, we use thermal baths on $\psi = 0$ and $\psi = 1$, and thus, we can impose an initial temperature gradient length $\kappa_T = 0.15$ and an initial density gradient length $\kappa_n = 0.05$. We also impose the electric potential to be 0 at the edges. Imposing such constraints usually creates numerical error when approaching the edges, and thus, we create an artificial diffusion, "buffers," between $\psi \in [0; 0.15]$ and $\psi \in [0.85; 1]$.[32] The ion Larmor radius is $\rho_i = 0.001$ and the ion banana width is $\delta_{bi} = 0.01$ which are given in units of ψ, at the thermal velocity, using the approximation of constant orbits. The initial electrostatic potential is a sum of sines both in α and ψ with random phases, and we choose the equilibrium ion distribution function f_{eq} as locally Maxwellian (exponential in E)

$$f_{eq}(\psi, E) = e^{-E}[1 + \psi(\kappa_T(E - 3/2) + \kappa_n)]. \tag{5}$$

We recall the input parameters in Table II.

With the goal of studying the test particle diffusion in a typical core plasma, we do not want zonal flows or streamers to be dominant because they would drastically enhance or reduce the radial transport of particles, and thus, it would not be a pertinent case to study the radial transport of test particles. We want a simulation with a global turbulence at the time of the study, where global means that there is no large electric potential structure either in ψ or in α. Figure 1 shows the time evolution of the 5 modes along with the 0th mode ($m = 0, 2, 4, 6, 7, 9$) in the α direction, in semilog. The mode magnitudes grow exponentially from $t = 0$ to $t \approx 2$, where the time t is normalized to the inverse precession frequency of particles with thermal velocity Ω_d^{-1}. Then, the modes reach the saturation level at $t \approx 2$, and nonlinear interactions are dominant. This is the turbulent phase where the modes are Trapped Ion Modes (TIMs). The 0th mode is not dominant throughout the simulation.

TABLE II. Input parameters.

Quantity	Value
Ion Larmor radius	$\rho_i = 0.001$
Ion banana width	$\delta_{bi} = 0.01$
Initial temperature gradient	$\kappa_T = 0.15$
Initial density gradient	$\kappa_n = 0.05$
Trapped particle precession frequency	$\Omega_d = 1$
C1	$C_1 = 0.1$
C2	$C_2 = 0.1$
Electron dissipation[31]	$\delta_m = 0.02$

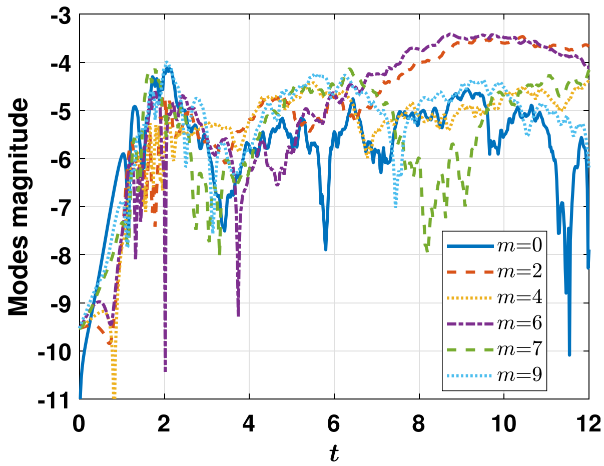

FIG. 1. Time-evolution of 5 α-modes, along with the 0th mode, in semilog at $\psi = 0.5$.

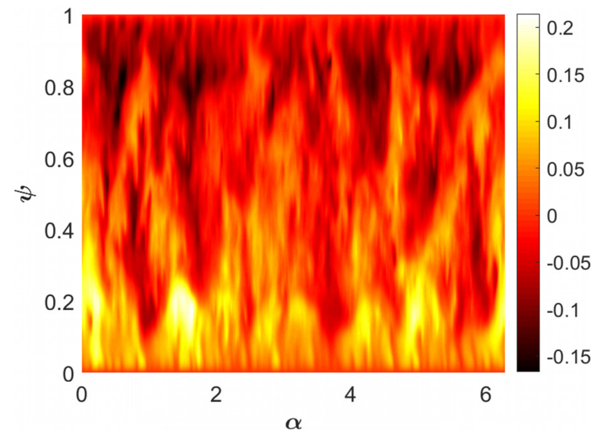

FIG. 3. Electric potential ϕ map at $t = 6$.

A global turbulence would not be dominated by large scale modes such as $k_{\alpha_m} L_\alpha \sim 1$ and $k_{\psi_n} L_\psi \sim 1$, where k_{α_m} and k_{ψ_n} are the mth and nth wavenumbers of a ϕ wave in (α, ψ) directions and $L_\alpha = 2\pi$ and $L_\psi = 1$ are the sizes of the box in α and ψ. Moreover, we would have a bulk of most intense α-modes (not the one dominant mode over the others) so that $\Delta m \sim \bar{m}$, where Δm is the mode range of the bulk of most intense α-modes and $\bar{m}$ the mean mode of this bulk. The autocorrelation time of the α-modes is $\tau_\alpha \approx 1$. The spectrum of α-modes averaged between $t = 6$ and $t = 7$ is shown in Fig. 2, and we can see that the mode range of the bulk of most intense α-modes is approximately $\Delta m \approx 10$, and the mean mode of this bulk of modes is $\bar{m} \approx 10$, so we do not have one very dominant mode but rather a collection of dominant modes of about the same amplitude.

Therefore, we choose to study the test particle diffusion at time $t = 6$. At this time, we have a ratio $e\phi/T \sim 0.01 - 0.03$, Fig. 3, which is typical in core fusion plasma.

We choose to initialize the test particles at time $t = 6$, with a Gaussian distribution in ψ centered in $\psi = 0.5$ and with a standard deviation $\Delta\psi = 0.022$, in order to minimize the sensitivity to the radial variations of turbulence. In the α direction, the test particles are distributed randomly. They have a fixed E. Figure 4 shows the test particle distribution function in ψ, for $E = 1.74$, from initialization at $t = 6$ to $t = 6.5$. Section IV shows that the highest rate of test particle radial transport is observed for $E = 1.74$. For each E, we use 10^6 test particles: 1000×1000 in the ψ and α directions.

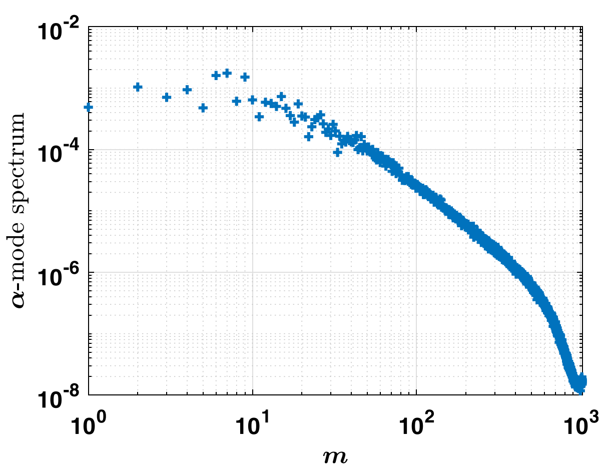

FIG. 2. Log-log spectrum of the α-modes at $\psi = 0.5$ and averaged over $t \in [6, 7]$.

IV. TEST PARTICLE DYNAMICS IN A TURBULENT PLASMA SIMULATION

In this section, we aim at developing a robust method for dissociating radial diffusion and radial convection of the test particles. We first study the time-evolution of the test particle Mean Squared Displacement (MSD) in the radial direction ψ for each E as they evolve in a turbulent plasma simulation. It allows us to estimate the turbulent radial diffusion coefficient in velocity space. We then find the radial

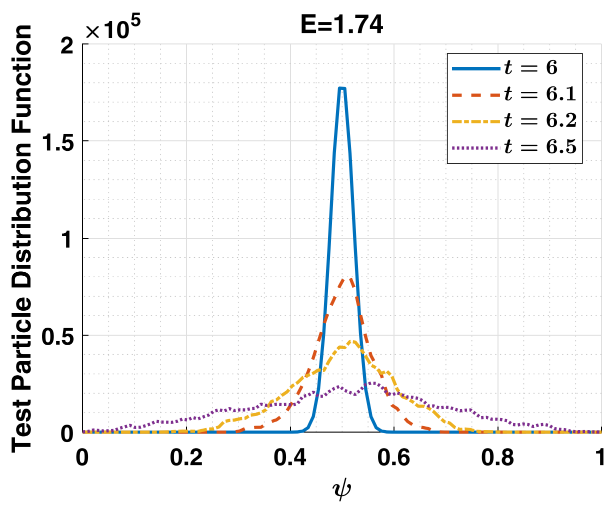

FIG. 4. Snapshot of the test particle distribution function from Gaussian initialization at $t = 6$ to $t = 6.5$, for $E = 1.74$.

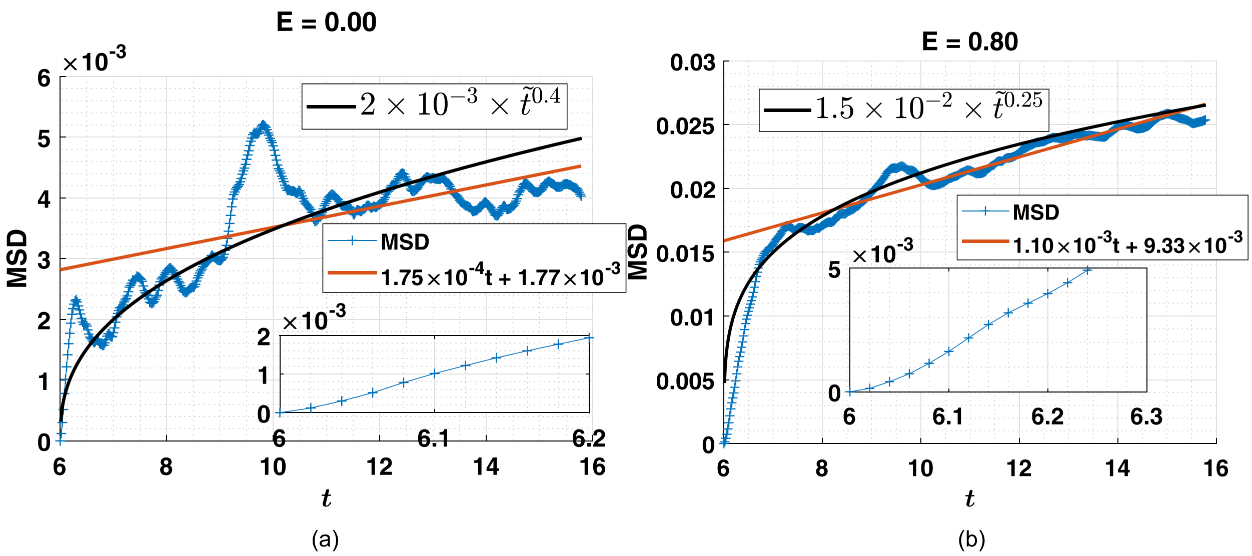

FIG. 5. Time evolution of the test particle MSD for $E = 0$ [5(a)] and $E = 0.8$ [5(b)]. In red is the linear fit of the MSD in phase 3 (diffusive phase). In black is the power law fit for all the simulation time, with $\tilde{t} = t - t_0$.

diffusive flux of the test particles, and we compare it to the total radial particle flux accounting for all the transport processes.

A. Estimation of a random walk radial diffusion coefficient in velocity space for the test particles

We let the test particles evolve in the turbulent simulation starting from time $t_0 = 6$. At each time step of the simulation, TERESA calculates the MSD of the test particles in the radial direction, where the average is over all the test particles: $\langle(\psi(t) - \psi(t_0))^2\rangle$, for each energy E. Later, we will see that around $E \approx 1.74$, there is a resonance between trapped ions and TIM, and therefore, we plot the time-evolution of this MSD for $E = 0$, $E = 0.8$, $E = 1.74$, $E = 2.71$, and $E = 3.2$, respectively, in Figs. 5(a), 5(b), 6(a), 6(b), and 7. For each E, we can distinguish different phenomena in time for the MSD. When the MSD grows linearly in time, we superpose the slope in red to the plot, and we will be able to calculate the diffusion coefficient.

In the general case, we expect the MSD to have 4 different phases at different time and space scales:

1. Phase 1: A first, rapid ($\sim 0.1\Omega_d^{-1}$) phase of local convection where the test particles reorganize themselves inside the local potential structure where they have been initialized in, typically on a space scale of 10^{-2} in units of ψ.

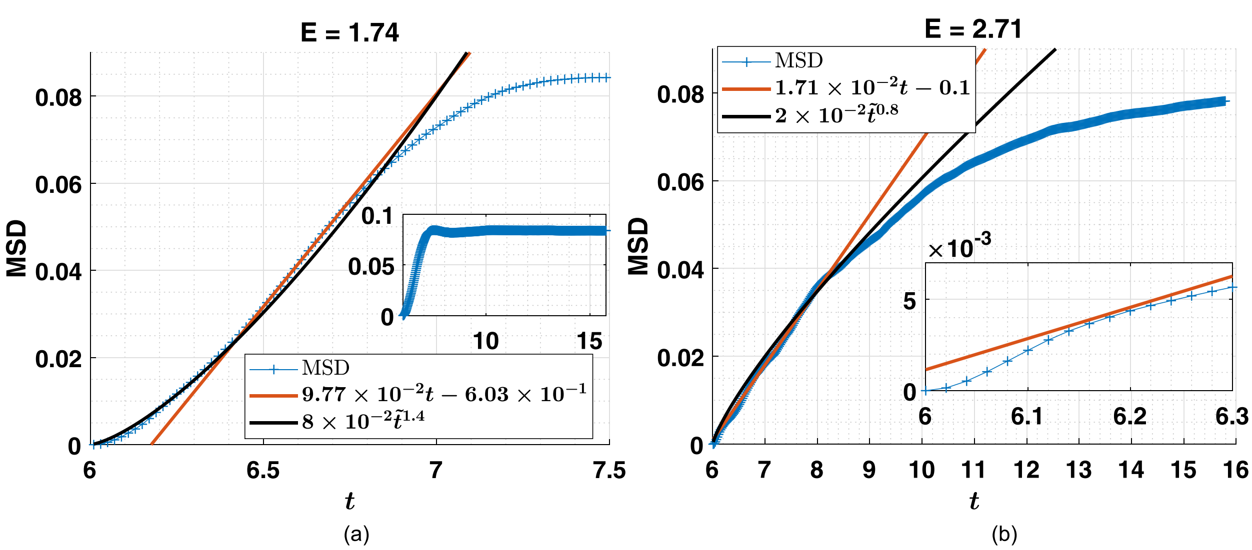

FIG. 6. Time evolution of the test particle MSD for $E = 1.74$ [6(a)] and $E = 2.71$ [6(b)]. In red is the linear fit of the MSD in phase 3 (diffusive phase). In black is the power law fit for all the simulation time, with $\tilde{t} = t - t_0$.

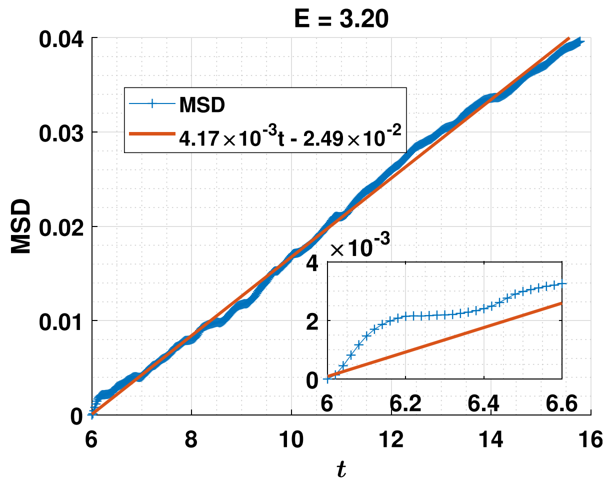

FIG. 7. Time evolution of the test particle MSD for $E = 3.2$. In red is the linear fit of the MSD in phase 3.

2. Phase 2: A phase of fast-diffusion ($\sim 0.2\Omega_d^{-1}$), on a space scale of $10^{-2} - 10^{-1}$ in units of ψ.
3. Phase 3: In this phase, the evolution of the MSD is somewhat complex, with strong fluctuations on a $\sim 0.1\Omega_d^{-1}$ timescale, indicating that the particle motion is not a simple combination of diffusion and convection on this timescale. However, on a timescale $\sim\Omega_d^{-1}$, of the order of the turbulent autocorrelation time, the MSD grows roughly linearly in time, on the space scale of the simulation box. Therefore, transport may be modeled by a simple diffusive process on this longer timescale. We thus make a linear fit on phase 3, which we superpose in red to the plot, to find the diffusive coefficient.
4. Phase 4: A phase of saturation due to nonlocal effects and boundary conditions, where the test particles have explored the whole simulation box in ψ and the MSD reaches a plateau at MSD ≈ 0.08.

For $E = 0$, see Fig. 5(a), the trapped particles have no kinetic energy in the α direction. Phase 1 is from $t = 6$ to $t \approx 6.1$, where the MSD grows quadratically with time until MSD $\approx 10^{-3}$. Phase 2 appears from $t \approx 6.1$ to $t \approx 6.3$ where the MSD grows to MSD $\approx 2.3 \times 10^{-3}$. Phase 3 is from $t \approx 6.3$ to the end of the simulation. Phase 4 does not appear on this figure, but the MSD would reach the saturation phase if the total simulation time were approximately one order of magnitude longer.

$E = 0.8$, Fig. 5(b), is an intermediary case. Phase 1 is present from $t = 6$ to $t \approx 6.1$, where the MSD grows quadratically with time until MSD $\approx 10^{-4}$. Phase 2 appears from $t \approx 6.1$ to $t \approx 6.7$ where the MSD grows to MSD $\approx 1.5 \times 10^{-2}$. Phase 3 is from $t \approx 6.3$ to the end of the simulation and is where we fit linearly the MSD. Phase 4 is again not present, for the same reason as before.

For $E = 1.74$, see Fig. 6(a), the test particles resonate with the TIM. Phase 1 is from $t \approx 6$ to $t \approx 6.4$. Phase 2 does not appear as the MSD transitions directly to phase 3. Phase 3 is from $t \approx 6.4$ to $t \approx 6.8$ where the MSD grows, linearly in time, from MSD ≈ 0.02 to MSD ≈ 0.06, as the test particles diffuse rapidly in ψ. Phase 4 appears from $t \approx 6.8$ to the end of the simulation, where the test particles have explored the whole simulation box in ψ and the MSD reaches a plateau at MSD ≈ 0.08.

At $E = 2.7$, Fig. 6(b), the test particles are above the resonance energy and have a higher $\dot{\alpha}$ than the precedent cases. Phase 1 is from $t \approx 6$ to $t \approx 6.1$. Phase 2 does not appear as the MSD directly enters phase 3 from $t \approx 6.1$ to $t \approx 8$, with the MSD growing linearly from MSD $\approx 10^{-3}$ to MSD ≈ 0.04. Then, the MSD enters phase 4 as the test particles are subject to boundary effects, finally reaching a plateau at MSD ≈ 0.08 at the end of the simulation.

For $E = 3.2$, Fig. 7, the test particles first explore the potential structure they were initialized in, in phase 1, from $t = 6$ to $t \approx 6.1$. Then, the MSD directly enters phase 3 as the test particles follow Brownian motion and the MSD grows linearly, until the end of the simulation. Phase 4 does not appear during the simulation time although the saturation would appear with a longer simulation (around $t \approx 20 - 30$).

From the MSD at each E, we calculate the slope of the MSD in phase 3, and thus, we can estimate a radial random walk diffusion coefficient of the test particles in E space (or velocity space), Fig. 8.

The diffusion coefficient has a peak ($D_{RW} \approx 5.2 \times 10^{-2}$) around the resonance energy $E_R \approx 1.74$ because at this E, the test particles tend to move simultaneously with the electric potential and thus diffuse in the radial direction much faster than at other E.

For high E, the test particles have a high velocity $\dot{\alpha}$ compared to the evolution of the electric potential and tend to perceive only an average of ϕ along their trajectories, and thus, their radial diffusion coefficient is much smaller.

To confirm that the diffusion coefficient calculated from the MSD is not spuriously influenced by convection, we analyze the standard deviation of the ψ-distribution of test particles, which cannot be influenced by convection. We find that there is no significant difference between the time-evolution of the variance and that of the MSD, except for a constant shift due to a finite initial standard deviation, which has no impact on the slope. Therefore, this second method of analysis, which unambiguously discriminate convection and diffusion, confirms the results of the first method. This agreement indicates that, on a time scale of the order of the turbulence autocorrelation time, transport is predominantly diffusive in this simulation.

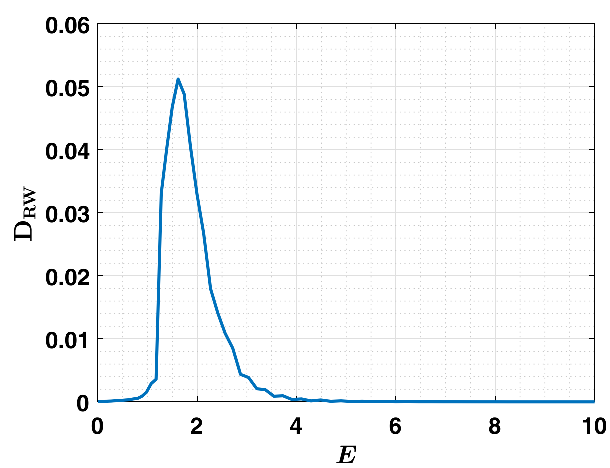

FIG. 8. Random walk radial diffusion coefficient in velocity space evaluated from the motion of the test particles.

We have interpreted the results in terms of a purely diffusive phase, in general preceded by a first phase of local convection and a second phase of fast-diffusion, followed by a phase of saturation due to the nonlocal effects and boundary conditions. However, the same results can also be interpreted in terms of a generalized $\langle(\psi(t)-\psi(t_0))^2\rangle = D(t-t_0)^p$ law, where $p<1$ and $p>1$ correspond to subdiffusion and superdiffusion. Figures 5 and 6 include fits to this generalized law. These fits indicate that transport is subdiffusive for particles outside the resonance energy and below high energies, Figs. 5 and 6(b), is superdiffusive for particles around the resonance energy, Fig. 6(a), and diffusive for high energies, Fig. 7.

Although we provide this alternative interpretation, the following analysis focuses on our first interpretation of a purely diffusive phase.

B. Comparison between the radial diffusion flux of the test particles and the total radial particle flux, in velocity space

From the random walk diffusion coefficient, we can estimate a radial diffusive flux for the test particles as

$$\Gamma_{\mathrm{D_{RW}}} = -\mathrm{D_{RW}}\left\langle \frac{\partial \langle f\rangle_\alpha}{\partial \psi}\right\rangle_{\psi\in[0.4;0.6]}, \tag{6}$$

where we averaged the radial gradient of $\langle f\rangle_\alpha$ over $\psi \in [0.4;0.6]$ in order to smooth out the local high variations of f in the radial direction. The diffusive flux $\Gamma_{\mathrm{D_{RW}}}$ is equal to the particle flux if transport is purely diffusive.

In Fig. 9, we compare the diffusive flux in blue to the total flux in red obtained directly from the TERESA code as

$$\Gamma_{\mathrm{Total}} = \langle \dot{\psi} f\rangle_\alpha, \tag{7}$$

which includes all radial transport processes such as diffusion or advection and which we average over $\psi \in [0.4;0.6]$ and over an autocorrelation time $t \in [6;7]$. We find that the radial particle transport is dominated by the resonant particle around the energy $E_R \approx 1.74$ where the trapped ions resonate with the TIM. As the peaks of the total flux and the diffusive flux are of the same magnitude, we can say that the transport of resonant particles is exclusively diffusive, following a random walk process, and moreover that the whole radial particle transport is dominated by diffusive processes. This is coherent with our choice of global turbulence as we chose to favor a turbulence driven by a bulk of the dominant TIM, with a nondominant large potential structure. Both flux peaks are negative (directed toward the edges) which is coherent with the gradient $\langle\frac{\partial\langle f\rangle_\alpha}{\partial\psi}\rangle_{\psi\in[0.4;0.6]}$ being positive at $E=E_R$, recalling that $\psi=1$ is toward the core and $\psi=0$ is toward the edge.

For high E and thus high $\dot{\alpha}$, the particle radial transport tends to be negligible, and thus, the two fluxes tend to 0, as explained in Sec. IV A.

For $E<1$, the gradient $\langle\frac{\partial\langle f\rangle_\alpha}{\partial\psi}\rangle_{\psi\in[0.4;0.6]}$ is negative, and thus, the diffusive flux is slightly positive (directed toward the core). The total flux is of the same sign as the diffusive flux, and thus, they are in the same direction. Between $E=0$ and $E\approx 0.5$, the total flux is a little less intense than the diffusive flux, indicating that the total flux may have a significant nondiffusive component directed toward the edge, although the discrepancy may be due to the uncertainty in measuring the slope of the MSD. Between $E\approx 0.5$ and $E\approx 1$, the total flux is more intense than the diffusive flux, indicating that the total flux may have a nondiffusive component in the same direction than the diffusive flux, i.e., directed toward the core. The use of test particles thus allows us to estimate the diffusive part of the flux in the total particle flux.

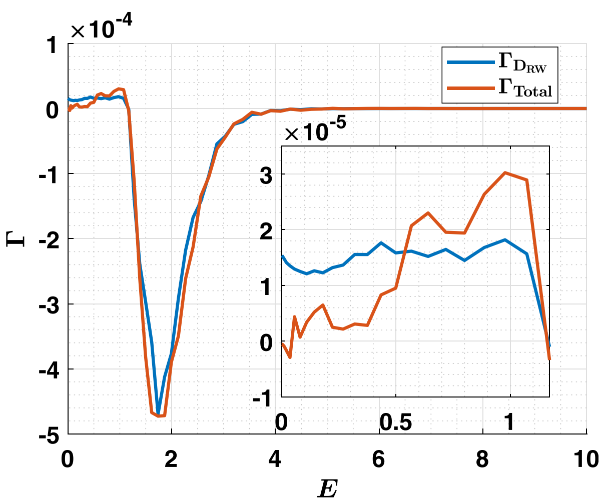

FIG. 9. Radial diffusion flux of the test particles (in blue) in velocity space, compared to the total flux given by the gyrokinetic simulation in red.

V. CONCLUSION

We added a test particle module to the reduced bounce-averaged gyrokinetic code TERESA which is focused on investigating the low frequency phenomena of the order of the trapped particles' toroidal precession frequency. The code can henceforth solve, in addition to the distribution function f and the electric potential ϕ, the individual trajectories of millions of test particles. The test particle positions in phase space are computed directly in the code, thus allowing the same order of accuracy than the TERESA numerical scheme. Test particles are particles which respond to the electrostatic field without contributing to it. The addition of test particles in our code gives us access to information which was not available before with only f and ϕ. It allows us to have better insights into the transport phenomena such as diffusion, advection, or ballistic motions.

In this first work, using test particles in TERESA, we aimed at separating the contribution of the diffusive process of the particles in the radial direction, from the total radial transport. To proceed, we initialized one million test particles at $t=6$, in a turbulent core plasma, in the center of our box ($\psi=0.5$) and let them evolve in the electrostatic potential. The turbulence is TIM-driven, and there are no dominant zonal flows, streamers, or large potential structures which would drastically impact the transport. Instead, the α-mode spectrum presents a bulk of most intense modes ranging from $m\approx 1$ to $m\approx 10$, and the ratio $e\phi/T \sim 0.01-0.03$ is typical of core turbulence.

We then calculated the time evolution of the test particle Mean Squared Displacement in the radial (ψ) direction, for each $E\in[0;20]$, and observed that the MSD tends to first have a rapid growth, indicating that the test particles reorganize themselves inside the potential structure where they were initialized in. Then, the test particle MSD grows linearly, indicating a radial diffusion process toward the edges of the box until the test particles start to undergo boundary effects. At $E_R = 1.74$ which is approximate when the particles resonate with the TIM, the MSD becomes constant in time at MSD $\approx$0.08, indicating that the test particles fully explored the box in the radial direction. At the resonant energy, the particles tend to "see" the constant potential structure and thus explore the simulation box faster than at nonresonant energies.

With the MSD obtained for each E, we calculated a radial random walk diffusion coefficient, which presents a peak around the resonant energy $E_R \approx 1.74$.

Then, we estimated the radial diffusive flux of the particles which is the flux if there was only a diffusion process. We compared it to the total flux obtained directly from the TERESA simulation accounting all the radial transport processes. We found that the radial particle transport is clearly dominated by the resonant particles, as both fluxes present a peak around $E_R \approx 1.74$. Both peaks are negative and of the same intensity, indicating that the radial transport of resonant particles is exclusively a diffusive process toward the edge. It is coherent with our choice of global turbulence. The high energy particle radial transport tends to be negligible. Below the resonance, for $E < 1$, the gradient of f is negative, and the diffusive flux is oriented toward the core. Between $E = 0$ and $E \approx 0.5$, there might be a nondiffusive process, directed toward the edge so that the total flux is lower than the diffusive flux. Between $E \approx 0.5$ and $E \approx 1$, a nondiffusive process appears to induce a flux directed toward the edge, so that the total flux is more intense than the diffusive flux.

This analysis was made in a broad spectrum ($\Delta m \sim \bar{m}$) turbulence. In a peaked ($\Delta m \ll \bar{m}$) spectrum turbulence, large radial structures (streamerlike) appear and the test particle transport is enhanced, so that $\Gamma_{D_{RW}}$ is one order of magnitude smaller than Γ_{Total} and the two fluxes are not peaked at a resonance energy anymore.

ACKNOWLEDGMENTS

This work was granted access to the HPC resources of IDRIS under the allocation 2017-27862 made by GENCI (Grand Equipement National de Calcul Intensif).

This work was carried out within the framework of the EUROfusion Consortium and French Research Federation for Fusion Studies and received funding from the Euratom research and training programme 2014–2018 under Grant Agreement No. 633053. The views and opinions expressed herein do not necessarily reflect those of the European Commission.

REFERENCES

[1]J. A. Boedo, G. D. Porter, M. J. Schaffer, R. Lehmer, R. A. Moyer, J. G. Watkins, T. E. Evans, C. J. Lasnier, A. W. Leonard, and S. L. Allen, "Flow reversal, convection, and modeling in the DIII-D divertor," Phys. Plasmas **5**(12), 4305–4310 (1998).
[2]J. A. Boedo, D. Rudakov, R. Moyer, S. Krasheninnikov, D. Whyte, G. McKee, G. Tynan, M. Schaffer, P. Stangeby, P. West *et al.*, "Transport by intermittent convection in the boundary of the DIII-D tokamak," Phys. Plasmas **8**(11), 4826–4833 (2001).
[3]A. J. Brizard and T. S. Hahm, "Foundations of nonlinear gyrokinetic theory," Rev. Mod. Phys. **79**(2), 421 (2007).
[4]J. Candy and R. E. Waltz, "Anomalous transport scaling in the DIII-D tokamak matched by supercomputer simulation," Phys. Rev. Lett. **91**(4), 045001 (2003).
[5]J. Candy and R. E. Waltz, "An Eulerian gyrokinetic-Maxwell solver," J. Comput. Phys. **186**(2), 545–581 (2003).
[6]T. Cartier-Michaud, P. Ghendrih, Y. Sarazin, G. Dif-Pradalier, T. Drouot, D. Estève, X. Garbet, V. Grandgirard, G. Latu, C. Norscini *et al.*, "Staircase temperature profiles and plasma transport self-organisation in a minimum kinetic model of turbulence based on the trapped ion mode instability," J. Phys.: Conf. Ser. **561**(1), 012003 (2014).
[7]T. Cartier-Michaud, P. Ghendrih, V. Grandgirard, and G. Latu, "Optimizing the parallel scheme of the poisson solver for the reduced kinetic code TERESA," ESAIM: Proc. **43**, 274–294 (2013).
[8]G. Darmet, Ph. Ghendrih, Y. Sarazin, X. Garbet, and V. Grandgirard, "Intermittency in flux driven kinetic simulations of trapped ion turbulence," Commun. Nonlinear Sci. Numer. Simul. **13**(1), 53–58 (2008).
[9]D. del Castillo-Negrete, P. Mantica, V. Naulin, J. Juul Rasmussen *et al.*, "Fractional diffusion models of non-local perturbative transport: Numerical results and application to jet experiments," Nucl. Fusion **48**(7), 075009 (2008).
[10]G. Depret, X. Garbet, P. Bertrand, and A. Ghizzo, "Trapped-ion driven turbulence in tokamak plasmas," Plasma Phys. Controlled Fusion **42**(9), 949 (2000).
[11]G. Dif-Pradalier, P. H. Diamond, V. Grandgirard, Y. Sarazin, J. Abiteboul, X. Garbet, Ph. Ghendrih, A. Strugarek, S. Ku, and C. S. Chang, "On the validity of the local diffusive paradigm in turbulent plasma transport," Phys. Rev. E **82**(2), 025401 (2010).
[12]G. Dif-Pradalier, V. Grandgirard, Y. Sarazin, X. Garbet, and Ph. Ghendrih, "Interplay between gyrokinetic turbulence, flows, and collisions: Perspectives on transport and poloidal rotation," Phys. Rev. Lett. **103**(6), 065002 (2009).
[13]W. Dorland, F. Jenko, M. Kotschenreuther, and B. N. Rogers, "Electron temperature gradient turbulence," Phys. Rev. Lett. **85**(26), 5579 (2000).
[14]T. Drouot, "Étude de la turbulence liée aux particules piégées dans les plasmas de fusion," Ph.D. thesis (Université de Lorraine, 2015).
[15]T. Drouot, E. Gravier, T. Reveille, M. Sarrat, M. Collard, P. Bertrand, T. Cartier-Michaud, P. Ghendrih, Y. Sarazin, and X. Garbet, "Global gyrokinetic simulations of trapped-electron mode and trapped-ion mode microturbulence," Phys. Plasmas **22**(8), 082302 (2015).
[16]D. Estève, Y. Sarazin, X. Garbet, V. Grandgirard, S. Breton, P. Donnel, Y. Asahi, C. Bourdelle, G. Dif-Pradalier, C. Ehrlacher *et al.*, "Self-consistent gyrokinetic modeling of neoclassical and turbulent impurity transport," Nucl. Fusion **58**(3), 036013 (2018).
[17]X. Garbet, P. Mantica, C. Angioni, E. Asp, Y. Baranov, C. Bourdelle, R. Budny, F. Crisanti, G. Cordey, L. Garzotti *et al.*, "Physics of transport in tokamaks," Plasma Phys. Controlled Fusion **46**(12B), B557 (2004).
[18]X. Garbet, Y. Idomura, L. Villard, and T. H. Watanabe, "Gyrokinetic simulations of turbulent transport," Nucl. Fusion **50**(4), 043002 (2010).
[19]A. Ghizzo, D. Del Sarto, X. Garbet, and Y. Sarazin, "Streamer-induced transport in the presence of trapped ion modes in tokamak plasmas," Phys. Plasmas **17**(9), 092501 (2010).
[20]T. Goerler, X. Lapillonne, S. Brunner, T. Dannert, F. Jenko, F. Merz, and D. Told, "The global version of the gyrokinetic turbulence code gene," J. Comput. Phys. **230**(18), 7053–7071 (2011).
[21]V. Grandgirard, Y. Sarazin, P. Angelino, A. Bottino, N. Crouseilles, G. Darmet, G. Dif-Pradalier, X. Garbet, P. Ghendrih, S. Jolliet *et al.*, "Global full-f gyrokinetic simulations of plasma turbulence," Plasma Phys. Controlled Fusion **49**(12B), B173 (2007).
[22]V. Grandgirard, M. Brunetti, P. Bertrand, N. Besse, X. Garbet, P. Ghendrih, G. Manfredi, Y. Sarazin, O. Sauter, E. Sonnendrücker *et al.*, "A drift-kinetic semi-Lagrangian 4D code for ion turbulence simulation," J. Comput. Phys. **217**(2), 395–423 (2006).
[23]R. W. Harvey, O. Sauter, R. Prater, and P. Nikkola, "Radial transport and electron-cyclotron-current drive in the TCV and DIII-D tokamaks," Phys. Rev. Lett. **88**(20), 205001 (2002).
[24]J. A. Heikkinen, S. Henriksson, S. Janhunen, T. P. Kiviniemi, and F. Ogando, "Gyrokinetic simulation of particle and heat transport in the presence of wide orbits and strong profile variations in the edge plasma," Contrib. Plasma Phys. **46**(7–9), 490–495 (2006).
[25]Y. Idomura, M. Ida, T. Kano, N. Aiba, and S. Tokuda, "Conservative global gyrokinetic toroidal full-f five-dimensional Vlasov simulation," Comput. Phys. Commun. **179**(6), 391–403 (2008).

[26]Y. Idomura, H. Urano, N. Aiba, and S. Tokuda, "Study of ion turbulent transport and profile formations using global gyrokinetic full-f Vlasov simulation," Nucl. Fusion **49**(6), 065029 (2009).
[27]M. B. Isichenko, A. V. Gruzinov, and P. H. Diamond, "Invariant measure and turbulent pinch in tokamaks," Phys. Rev. Lett. **74**(22), 4436 (1995).
[28]F. Jenko, W. Dorland, M. Kotschenreuther, and B. N. Rogers, "Electron temperature gradient driven turbulence," Phys. Plasmas **7**(5), 1904–1910 (2000).
[29]S. Jolliet, A. Bottino, P. Angelino, R. Hatzky, T. M. Tran, B. F. Mcmillan, O. Sauter, K. Appert, Y. Idomura, and L. Villard, "A global collisionless PIC code in magnetic coordinates," Comput. Phys. Commun. **177**(5), 409–425 (2007).
[30]J.-M. Kwon, W. Horton, P. Zhu, P. J. Morrison, H.-B. Park, and D. I. Choi, "Global drift wave map test particle simulations," Phys. Plasmas **7**(4), 1169–1180 (2000).
[31]M. Lesur, T. Cartier-Michaud, T. Drouot, P. H. Diamond, Y. Kosuga, T. Reveille, E. Gravier, X. Garbet, S.-I. Itoh, and K. Itoh, "A simple model for electron dissipation in trapped ion turbulence," Phys. Plasmas **24**(1), 012511 (2017).
[32]J. Médina, M. Lesur, E. Gravier, T. Réveillé, M. Idouakass, T. Drouot, P. Bertrand, T. Cartier-Michaud, X. Garbet, and P. H. Diamond, "Radial density and heat fluxes description in the velocity space: Nonlinear simulations and quasi-linear calculations," Phys. Plasmas **25**(12), 122304 (2018).
[33]T. M. Minea, C. Costin, A. Revel, D. Lundin, and L. Caillault, "Kinetics of plasma species and their ionization in short-hipims by particle modeling," Surf. Coat. Technol. **255**, 52–61 (2014).
[34]A. G. Peeters, Y. Camenen, F. James Casson, W. A. Hornsby, A. P. Snodin, D. Strintzi, and G. Szepesi, "The nonlinear gyro-kinetic flux tube code GKW," Comput. Phys. Commun. **180**(12), 2650–2672 (2009).
[35]A. B. Rechester and M. N. Rosenbluth, "Electron heat transport in a tokamak with destroyed magnetic surfaces," Phys. Rev. Lett. **40**(1), 38 (1978).
[36]R. Sanchez and D. E. Newman, "Self-organized criticality and the dynamics of near-marginal turbulent transport in magnetically confined fusion plasmas," Plasma Phys. Controlled Fusion **57**(12), 123002 (2015).
[37]R. Sanchez, D. E. Newman, J.-N. Leboeuf, V. K. Decyk, and B. A. Carreras, "Nature of transport across sheared zonal flows in electrostatic ion-temperature-gradient gyrokinetic plasma turbulence," Phys. Rev. Lett. **101**(20), 205002 (2008).
[38]R. Sanchez, D. E. Newman, J. N. Leboeuf, and V. K. Decyk, "Nature of turbulent transport across sheared zonal flows: Insights from gyrokinetic simulations," Plasma Phys. Controlled Fusion **53**(7), 074018 (2011).
[39]Y. Sarazin, V. Grandgirard, J. Abiteboul, S. Allfrey, X. Garbet, Ph. Ghendrih, G. Latu, A. Strugarek, G. Dif-Pradalier, P. H. Diamond *et al.*, "Predictions on heat transport and plasma rotation from global gyrokinetic simulations," Nucl. Fusion **51**(10), 103023 (2011).
[40]Y. Sarazin, V. Grandgirard, E. Fleurence, X. Garbet, P. Ghendrih, P. Bertrand, and G. Depret, "Kinetic features of interchange turbulence," Plasma Phys. Controlled Fusion **47**(10), 1817 (2005).
[41]Y. Sarazin, V. Grandgirard, J. Abiteboul, S. Allfrey, X. Garbet, Ph. Ghendrih, G. Latu, A. Strugarek, and G. Dif-Pradalier, "Large scale dynamics in flux driven gyrokinetic turbulence," Nucl. Fusion **50**(5), 054004 (2010).
[42]G. Spizzo, R. White, M. Maraschek, V. Igochine, G. Granucci *et al.*, "Nonlocal transport in toroidal plasma devices," Nucl. Fusion **59**(1), 016019 (2019).
[43]B. Ph. V. Milligen, B. A. Carreras, and R. Sanchez, "The foundations of diffusion revisited," Plasma Phys. Controlled Fusion **47**(12B), B743 (2005).
[44]D. Wünderlich, L. Schiesko, P. McNeely, U. Fantz, P. Franzen *et al.*, "On the proton flux toward the plasma grid in a RF-driven negative hydrogen ion source for ITER NBI," Plasma Phys. Controlled Fusion **54**(12), 125002 (2012).
[45]G. M. Zaslavsky and G. Moiseevič Zaslavskij, *Hamiltonian Chaos and Fractional Dynamics* (Oxford University Press on Demand, 2005).